# Numerically solvable model for resonant collisions of electrons with diatomic molecules

Karel Houfek* and T. N. Rescigno[†]

*Chemical Sciences, Lawrence Berkeley National Laboratory, Berkeley, California 94720, USA*

C. W. McCurdy[‡]

*Department of Applied Science and Department of Chemistry, University of California, Davis, California 95616, USA*
*and Chemical Sciences, Lawrence Berkeley National Laboratory, Berkeley, California 94720, USA*

We describe a simple model for electron-molecule collisions that has one nuclear and one electronic degree of freedom and that can be solved to arbitrarily high precision, without making the Born-Oppenheimer approximation, by employing a combination of the exterior complex scaling method and a finite-element implementation of the discrete-variable representation. We compare exact cross sections for vibrational excitation and dissociative attachment with results obtained using the local complex potential approximation as commonly applied in the "boomerang" model, and suggest how this two-dimensional model can be used to test the underpinnings of contemporary nonlocal approximations to resonant collisions.

PACS number(s): 34.80.Ht, 34.80.Gs

## I. INTRODUCTION

For decades, resonant collisions of electrons with diatomic molecules have been studied with theoretical methods that seek to describe the nuclear dynamics of vibration or dissociation during the collision. The basic idea of these approaches is to cast the problem in terms effective potentials or effective Hamiltonians for nuclear motion that can be constructed, at least in principle, from an adiabatic (fixed-nuclei) description of the electron scattering resonance and its coupling to the electronic continuum.

Among the earliest work in this area is that of O'Malley [1,2] and O'Malley and Taylor [3] on dissociative attachment based on the idea of Feshbach partitioning of the electron scattering wave function into resonant and nonresonant parts. Herzenberg and co-workers [4–6] later applied these ideas to vibrational excitation and developed the local complex potential model that is generally known as the "boomerang model" in this context and that has been widely applied. More sophisticated approaches involving nonlocal, complex, and energy-dependent potentials for nuclear motion have been developed since then [7,8], and applied to a number of diatomic systems. The class of such methods based on projection operators was reviewed by Domcke in the early 1990s [9].

Judging from the comparison of the calculated cross sections with experiment, the nonlocal theories have been used with great success to describe both vibrational excitation and dissociative attachment to diatomic molecules, as can be seen from just a sampling of such studies [6–13]. However, in almost all cases the parameters of these calculations are found either by fitting some portion of the known experimental results, or in an approximate way from *ab initio* calculations, and they generally involve assumed forms for the coordinate and energy dependence of those parameters. Since a complete set of experimental measurements for all processes that can occur in these collisions is never available, it has been difficult to make a definitive test of the underlying assumptions of the formulation of the theory.

Our purpose here is to construct a theoretical laboratory in which such tests can be made unambiguously, including the question of whether non Born-Oppenheimer effects can be important in these resonant collisions—either within the resonant state or in the electronic continuum to which it couples. To that end we have constructed a two-dimensional model system, with one electronic and one nuclear degree of freedom. This two-dimensional problem can be solved to arbitrary precision by using a combination of two modern numerical methods. One of them is the exterior complex scaling (ECS) method, which allows us in this context to construct the full Green's function for this two-dimensional problem. The second is a generalization [14] of the discrete-variable representation (DVR) [15] which combines that idea with the finite-element method (FEM). The combination of these ideas has been used with great success in a different context to solve problems that involve two electrons in the continuum [16]. In this work it allows us to solve this model problem exactly for the processes of vibrational excitation,

$$e^- + AB(v_i) \rightarrow e^- + AB(v_f), \tag{1}$$

and dissociative electron attachment,

$$e^- + AB(v_i) \rightarrow A + B^-. \tag{2}$$

Here we show how this two-dimensional model can be designed to mimic some well-studied electron-molecule scattering problems that are dominated by shape resonances. The physics of the coupled electron-nuclear motion are visible in the exact wave functions we calculate for these systems.

---

*Permanent address: Institute of Theoretical Physics, Faculty of Mathematics and Physics, Charles University Prague, V Holešov-ičkách 2, 180 00 Praha 8, Czech Republic. Electronic address: khoufek@lbl.gov

[†]Electronic address: tnrescigno@lbl.gov

[‡]Electronic address: cwmccurdy@lbl.gov

Moreover, the cross sections are both qualitatively and quantitatively similar to those measured for the corresponding real systems.

The principal result we present here is the description of this model system and the exact behavior of the cross sections associated with it. Furthermore, we compare the exact cross sections with those calculated using two variants of the local complex potential approximation to this two-dimensional model. The comparison is unambiguous because we can define the local complex potential from the exact energy of the resonance pole of the $S$ matrix for scattering of the electron for a fixed internuclear distance.

These are the first steps toward comparing various nonlocal approximations to the dynamics of nuclear motion with the exact results to test their validity. Within this model we can construct the parameters of those approximations unambiguously in precise numerical calculations. Moreover we will argue that the fact that we can exactly calculate any aspect of the dynamics of this model problem will eventually allow us to separate the nonlocal effects that arise from coupling of electron scattering resonances to the continuum into which they can decay from effects due to the breakdown of the Born-Oppenheimer approximation that is generally made in the nonlocal theories.

In the following section we describe the two-dimensional model Hamiltonian and the definitions of the vibrational excitation and dissociative attachment cross sections in terms of the exact wave functions. In Sec. III we discuss the numerical methods used to solve this problem to arbitrary accuracy. In Sec. IV we describe the local complex potential approximation to the dynamics of this model system. In Sec. V we will discuss the choice of parameters with which this model can mimic the dynamics of electronic collisions with the $N_2$ and NO molecules and demonstrate that the physics of these collisions can be seen clearly in the resulting wave functions and cross sections. Finally in Sec. VI we will discuss briefly how this model can allow us to probe the underlying assumptions of the current theories of resonant collisions of electrons with molecules.

## II. GENERAL DESCRIPTION OF THE TWO-DIMENSIONAL MODEL

The Hamiltonian of our two-dimensional model with one nuclear and one electronic degree of freedom is

$$H = T_R + T_r + V(R,r) \tag{3}$$

where

$$T_R = -\frac{1}{2\mu}\frac{d^2}{dR^2}, \quad T_r = -\frac{1}{2}\frac{d^2}{dr^2} \tag{4}$$

are molecular and electronic kinetic energy operators, $\mu$ is the reduced mass of a molecule, $R$ is the internuclear distance and $r$ is the distance of the electron from the molecule. The potential $V(R,r)$ is chosen to have the form

$$V(R,r) = V_0(R) + \frac{l(l+1)}{2r^2} + V_{\text{int}}(R,r), \tag{5}$$

with

$$V_{\text{int}}(R,r) = -\lambda(R)e^{-\alpha(R)r^2}. \tag{6}$$

In Eq. (5) the potential $V_0(R)$ describes the vibrational motion of the neutral molecule and it is the limit of the full effective potential $V(R,r)$, when the electron is at infinity

$$\lim_{r\to\infty} V(R,r) = V_0(R). \tag{7}$$

The interaction of the electron with the molecule, Eq. (6), is determined by functions $\lambda(R)$ and $\alpha(R)$. Roughly speaking, $\lambda(R)$ controls the depth of the electronic potential well and $\alpha(R)$ determines the width of this well. The centrifugal term ($l$ denotes electron angular momentum) is present to provide resonant behavior in our model system for an overall attractive choice of the interaction potential. By diagonalizing the fixed-nuclei (electronic) Hamiltonian

$$H_{\text{el}} = T_r + V(R,r) \tag{8}$$

we get an adiabatic potential energy curve of the molecular anion $(AB)^-$.

With the Hamiltonian of Eq. (3), the system $e^- + AB$ at a given energy $E$ is described by the solution of the Schrödinger equation

$$H\Psi_E^+(R,r) = E\Psi_E^+(R,r) \tag{9}$$

where $\Psi_E^+(R,r)$ satisfies appropriate boundary conditions. Here we are especially interested in two inelastic processes, namely, vibrational excitation and dissociative attachment. The initial state of the model system for these two processes is the same and reads

$$\Psi_{v_i}^0(R,r) = \chi_{v_i}(R)rj_l(k_{\text{ei}}r). \tag{10}$$

$\chi_{v_i}(R)$ is a initial vibrational state of the molecule satisfying the equation

$$[T_R + V_0(R)]\chi_v(R) = E_v\chi_v(R) \tag{11}$$

and $j_l$ is a spherical Bessel function of the first kind [17] describing an incoming electron with momentum $k_{\text{ei}}$. The total energy of the system is

$$E = E_{v_i} + \frac{k_{\text{ei}}^2}{2}. \tag{12}$$

To solve Eq. (9), we partition the full wave function $\Psi_E^+$ into incident and scattered parts,

$$\Psi_E^+(R,r) = \Psi_{v_i}^0(R,r) + \Psi_{\text{sc}}(R,r). \tag{13}$$

The unknown scattered part of the wave function, $\Psi_{\text{sc}}(R,r)$, then satisfies a driven Schrödinger equation

$$(E - H)\Psi_{\text{sc}}(R,r) = V_{\text{int}}(R,r)\Psi_{v_i}^0(R,r), \tag{14}$$

the boundary conditions for which are

$$\Psi_{\text{sc}}(R,r) \xrightarrow[r\to\infty]{} \sum_{v_f} f_{v_i\to v_f}^{\text{VE}}\chi_{v_f}(R)rh_l^{(1)}(k_{\text{ef}}r), \tag{15}$$

$$\Psi_{\mathrm{sc}}(R,r) \xrightarrow[R\to\infty]{} f^{\mathrm{DA}}_{v_{\mathrm{i}}} \phi_{\mathrm{b}}(r) R h_0^{(1)}(K_{\mathrm{DA}}R) \qquad (16)$$

where $h_l^{(1)}$ is a spherical Hankel function [17]. The scattering amplitudes for vibrational excitation, $f^{\mathrm{VE}}_{v_{\mathrm{i}}\to v_{\mathrm{f}}}$, and for dissociative attachment, $f^{\mathrm{DA}}_{v_{\mathrm{i}}}$, are related to the $T$ matrices for these processes which we will define below.

The sum in Eq. (15) runs over all open vibrational excitation channels, for which $\chi_{v_{\mathrm{f}}}(R)$ is the final vibrational state of the molecule with energy $E_{v_{\mathrm{f}}}$ and $k_{\mathrm{ef}}$ denotes the final momentum of the electron. Equation (16) is the asymptotic condition for the dissociative attachment channel (if it is open). We suppose here that the model potential in Eq. (5) supports only one bound state, $\phi_{\mathrm{b}}(r)$, of the electron as $R \to \infty$,

$$\left(T_r + \frac{l(l+1)}{2r^2} + \lim_{R\to\infty} V_{\mathrm{int}}(R,r)\right)\phi_{\mathrm{b}}(r) = E_{\mathrm{b}}\phi_{\mathrm{b}}(r), \quad (17)$$

which is appropriate for both the $N_2$-like and NO-like models we will treat here. The binding energy $E_{\mathrm{b}}$ is related to the electron affinity $E_{\mathrm{a}}$ of the atom $B$ by $E_{\mathrm{a}}=-E_{\mathrm{b}}$. The relative momentum $K_{\mathrm{DA}}$ of $A$ and $B^-$ in the dissociative attachment channel is given by

$$E = \frac{K_{\mathrm{DA}}^2}{2\mu} + E_{\mathrm{b}}. \qquad (18)$$

Finally, we give the expressions for the cross sections in terms of the $T$ matrices defined for the vibrational excitation and dissociative attachment channels in terms of matrix elements of the interaction potentials,

$$T^{\mathrm{VE}}_{v_{\mathrm{i}}\to v_{\mathrm{f}}}(E) = \langle \Psi^0_{v_{\mathrm{f}}}|V_{\mathrm{VE}}|\Psi^+_E\rangle$$

$$= \int_0^\infty dR \int_0^\infty dr\, \Psi^0_{v_{\mathrm{f}}}(R,r) V_{\mathrm{VE}}(R,r) \Psi^+_E(R,r)$$

$$= \frac{f^{\mathrm{VE}}_{v_{\mathrm{i}}\to v_{\mathrm{f}}}(E)}{2k_{\mathrm{ef}}}, \qquad (19)$$

$$T^{\mathrm{DA}}_{v_{\mathrm{i}}}(E) = \langle \Psi^0_{\mathrm{DA}}|V_{\mathrm{DA}}|\Psi^+_E\rangle$$

$$= \int_0^\infty dR \int_0^\infty dr\, \Psi^0_{\mathrm{DA}}(R,r) V_{\mathrm{DA}}(R,r) \Psi^+_E(R,r) = \frac{f^{\mathrm{DA}}_{v_{\mathrm{i}}}(E)}{2\mu k_{\mathrm{DA}}}. \qquad (20)$$

The unperturbed final states in the vibrational excitation and dissociative attachment channels are given by

$$\Psi^0_{v_{\mathrm{f}}}(R,r) = \chi_{v_{\mathrm{f}}}(R) r j_l(k_{\mathrm{ef}}r), \qquad (21)$$

$$\Psi^0_{\mathrm{DA}}(R,r) = R j_0(K_{\mathrm{DA}}R)\phi_{\mathrm{b}}(r), \qquad (22)$$

the interaction potential in the vibrational excitation channel is the interaction between the electron and molecule, given in Eq. (6),

$$V_{\mathrm{VE}}(R,r) = V_{\mathrm{int}}(R,r) \qquad (23)$$

and in the dissociative attachment channel we define

$$V_{\mathrm{DA}}(R,r) = V_0(R) + V_{\mathrm{int}}(R,r) - \lim_{R\to\infty} V_{\mathrm{int}}(R,r). \qquad (24)$$

The resulting formulas for the cross sections can then be written as

$$\sigma^{\mathrm{VE}}_{v_{\mathrm{i}}\to v_{\mathrm{f}}}(E) = \frac{16\pi k_{\mathrm{ef}}}{k_{\mathrm{ei}}}|T^{\mathrm{VE}}_{v_{\mathrm{i}}\to v_{\mathrm{f}}}(E)|^2, \qquad (25)$$

$$\sigma^{\mathrm{DA}}_{v_{\mathrm{i}}}(E) = \frac{16\pi\mu K_{\mathrm{DA}}}{k_{\mathrm{ei}}}|T^{\mathrm{DA}}_{v_{\mathrm{i}}}(E)|^2. \qquad (26)$$

## III. NUMERICAL SOLUTION AND EVALUATION OF CROSS SECTIONS

### A. Numerical method

To solve Eq. (14) and to find bound states of the electron and molecule [Eqs. (11) and (17)] we have made use of the exterior complex scaling method implemented using finite elements with a discrete-variable representation basis introduced by Rescigno and McCurdy [14]. Details of this very efficient numerical representation, called the FEM DVR, together with a description of some of its previous applications, can be found in a recent review [16]. Here we only mention some of its main features and how they relate to the present study.

Employing the ECS method for both electronic, $r$, and nuclear, $R$, coordinates

$$R'(R) = \begin{cases} R, & R < R_0, \\ R_0 + (R-R_0)e^{i\eta_R}, & R \geqslant R_0, \end{cases} \qquad (27)$$

$$r'(r) = \begin{cases} r, & r < r_0, \\ r_0 + (r-r_0)e^{i\eta_r}, & r \geqslant r_0, \end{cases} \qquad (28)$$

we avoid the need for explicit imposition of asymptotic boundary conditions in vibrational excitation (an outgoing electron) and dissociative attachment (an outgoing atom and anion) channels. In the region where both coordinates are real, as illustrated in Fig. 1, the solution of Eq. (14) obtained by the ECS method is equal to the physical wave function of the system and all integrals defining the scattering amplitudes are evaluated in this region or on its boundary. Therefore the ECS radii $R_0$ and $r_0$ must be chosen large enough to contain all relevant interactions.

Because of the large difference between the masses of the electron and molecule we use different grids for the two coordinates $r$ and $R$. Moreover, in order to perform the two-dimensional calculations efficiently we adapted the $R$ grids to the molecular and molecular anion potentials of a particular model (the grid is much denser in the regions of deep potential wells). The nuclear grid typically consists of about 40-50 elements and the electron grid of 10-15 elements with 17 DVR basis functions in each element (Lagrange interpolating polynomials with mesh points derived from a Gauss-Lobatto quadrature). ECS was employed always for the electronic coordinate with $r_0=100$ but the nuclear coordinate has to be complex scaled only if the dissociative attachment
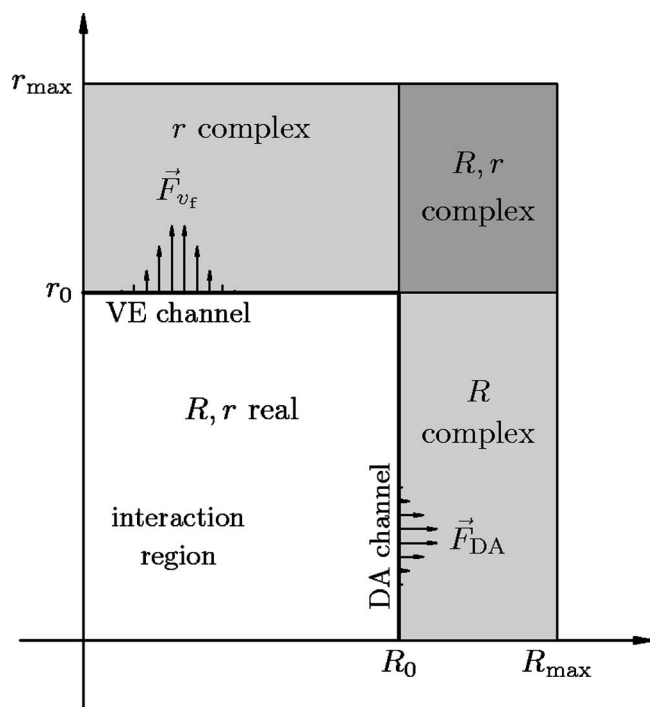
FIG. 1. Implementation of the ECS method for a system with one molecular ($R$) and one electronic ($r$) degree of freedom. Fluxes into vibrational excitation and dissociative attachment channels, which are integrated along the lines $r=r_0$ and $R=R_0$ in Eqs. (32) and (34) to calculate cross sections, are shown schematically.

channel is open (in the case of the NO-like model we set $R_0=12$).

A great advantage of the FEM DVR approach is that any local operator, like the potential energy in Eq. (5), has a diagonal representation. Although the kinetic energy is non-diagonal, its matrix elements have simple analytic forms, and because we use the DVR in combination with the finite-element method the resulting matrix representation of the full Hamiltonian of Eq. (3) is very sparse, usually having less than 0.05% nonzero elements. This sparse matrix is complex symmetric, and efficient standard numerical methods are available to solve the resulting matrix representation of Eq. (14).

### B. Evaluation of cross sections

Given the solution of the driven Schrödinger equation in Eq. (14) we need a procedure for extracting the cross sections for the collision processes we are interested in. Here we give two equivalent methods for evaluating the cross sections from the wave function computed on the grid, which we have used to test the stability and precision of the numerical methods employed to solve Eq. (14).

First, the cross section can be given in terms of the flux projected into a given final channel

$$\vec{F}_{\text{f}} = \frac{1}{2i}[(P_{\text{f}}\Psi_{\text{sc}})^* \nabla P_{\text{f}}\Psi_{\text{sc}} - \text{H.c.}] \qquad (29)$$

where the $P_{\text{f}}$ is a projection operator for the final channel, H.c. denotes the Hermitian conjugate, and the gradient operator in this case is

$$\nabla = \begin{pmatrix} \dfrac{1}{\mu}\dfrac{\partial}{\partial R} \\[2mm] \dfrac{\partial}{\partial r} \end{pmatrix}. \qquad (30)$$

In the vibrational excitation channel, $P_{\text{f}}=P_{v_{\text{f}}}$ projects on the final vibrational state

$$P_{v_{\text{f}}}\Psi_{\text{sc}}(R,r) = \chi_{v_{\text{f}}}(R) \int_0^\infty \chi_{v_{\text{f}}}^*(R')\Psi_{\text{sc}}(R',r)dR'. \qquad (31)$$

The cross section in terms of the projected flux reads

$$\sigma_{v_{\text{i}} \to v_{\text{f}}}^{\text{VE}}(E) = \frac{4\pi}{k_{\text{ei}}} \lim_{r\to\infty} \int_0^\infty \vec{F}_{v_{\text{f}}}(R,r) \cdot \vec{n}_r dR \qquad (32)$$

where $\vec{n}_r$ denotes a unit vector for the electronic coordinate $r$. Similarly, in the dissociative attachment channel we have the projection operator

$$P_{\text{DA}}\Psi_{\text{sc}}(R,r) = \phi_{\text{b}}(r) \int_0^\infty \phi_{\text{b}}^*(r')\Psi_{\text{sc}}(R,r')dr', \qquad (33)$$

and the corresponding cross section is

$$\sigma_{v_{\text{i}}}^{\text{DA}}(E) = \frac{4\pi}{k_{\text{ei}}} \lim_{R\to\infty} \int_0^\infty \vec{F}_{\text{DA}}(R,r) \cdot \vec{n}_R dr \qquad (34)$$

where $\phi_{\text{b}}(r)$ is defined by Eq. (17).

An alternative way to calculate these cross sections can be based on direct evaluation of the appropriate $T$-matrix elements using Eqs. (19) and (20), and the definition of the cross section in terms of them in Eqs. (25) and (26). We can evaluate the necessary integrals directly using the Gauss-Lobatto quadrature used to define the DVR basis, or we can transform the volume integrals in Eqs. (19) and (20) to surface integrals using Green's theorem. The $T$-matrix elements then take the form [16]

$$T(E) = \langle\Psi_{\text{f}}^0|V|\Psi_E^+\rangle = \langle\Psi_{\text{f}}^0|E - H^0|\Psi_{\text{sc}}\rangle$$

$$= \frac{1}{2}\int_S (\Psi_{\text{f}}^{0*} \nabla \Psi_{\text{sc}} - \Psi_{\text{sc}} \nabla \Psi_{\text{f}}^{0*}) \cdot d\hat{S} \qquad (35)$$

where $\nabla$ is defined in Eq. (30). In the case of vibrational excitation we use $V=V_{\text{VE}}$ from Eq. (23) so that $H^0=H-V_{\text{VE}}$ and $\Psi_{\text{f}}^0$ is given by Eq. (21), while for dissociative attachment the potential is $V_{\text{DA}}$ as defined in Eq. (24) and $\Psi_{\text{f}}^0$ is given by Eq. (22).

### IV. LOCAL COMPLEX POTENTIAL APPROXIMATION

To describe the nuclear dynamics of the negative molecular anion of a real system like $e^- + N_2$, one generally has to resort to approximate methods that are based on the Born-Oppenheimer approximation. The simplest and most frequently used approach is the local complex potential (LCP) approximation, which for vibrational excitation is also known as the boomerang model.

In this approach, we define the resonant molecular anion potential curve via the poles of the fixed-nuclei electron-

TABLE I. Parameters of the $N_2$- and NO-like models, given in atomic units, so that the resulting potential $V(R,r)$ is in hartrees.

| Parameter | $N_2$ | NO |
|---|---|---|
| $\mu$ | 12766.36 | 13614.16 |
| $l$ | 2 ($d$ wave) | 1 ($p$ wave) |
| $D_0$ | 0.75102 | 0.2363 |
| $\alpha_0$ | 1.15350 | 1.5710 |
| $R_0$ | 2.01943 | 2.1570 |
| $\lambda_\infty$ | 6.21066 | 6.3670 |
| $\lambda_1$ | 1.05708 | 5.0000 |
| $R_\lambda$ | −27.9833 | 2.0843 |
| $\lambda_c$ | 5.38022 | 6.0500 |
| $R_c$ | 2.40500 | 2.2850 |
| $\alpha_c$ | 0.40000 | 1.0000 |

scattering $S$ matrix, which can be obtained by finding bound or resonance energies of the electronic Hamiltonian in Eq. (8),

$$H_{el}(R)\varphi(r;R) = V_{res}(R)\varphi(r;R), \qquad (36)$$

$$V_{res}(R) = E_{res}(R) - \frac{i}{2}\Gamma(R), \qquad (37)$$

with all quantities depending parametrically on the internuclear distance $R$. Typically there is one bound electronic state of the molecular anion for large $R$, where $V_{res}(R)$ is real and less than $V_0(R)$. That bound state becomes a resonance state at internuclear distances shorter than some critical distance $R_c$ where the molecular anion potential energy curve crosses the potential energy curve $V_0(R)$ of the neutral molecule. For $R < R_c$ the anion potential $V_{res}(R)$ is complex and the real part $E_{res}(R) > V_0(R)$.

The dynamics of the temporary molecular anion state in the LCP approximation is described [6] by the equation

$$[E - T_R - V_{res}(R)]\xi_E(R) = \zeta_{v_i}(R)\chi_{v_i}(R), \qquad (38)$$

where $\zeta_{v_i}(R)$ is the so-called "entry amplitude" for capture of the electron into the resonant state with the molecule in the initial vibrational state $\chi_{v_i}(R)$. The numerical methods described in Sec. III can be used to obtain the adiabatic potential energy curve $V_{res}(R)$ defined by Eq. (36) and to solve Eq. (38).

The vibrational excitation and dissociative attachment cross sections are then given as

$$\sigma_{v_i \to v_f}^{VE}(E) = \frac{4\pi^3}{k_{ei}^2}\left|\int_0^\infty dR\, \chi_{v_f}^*(R)\zeta_{v_f}(R)\xi_E(R)\right|^2, \qquad (39)$$

$$\sigma_{v_i}^{DA}(E) = \frac{2\pi^2}{k_{ei}^2}\frac{K_{DA}}{\mu}\lim_{R\to\infty}|\xi_E(R)|^2 \qquad (40)$$

where $\zeta_{v_f}(R)$ is the so-called "exit amplitude."

In the standard LCP approximation, the entry and exit amplitudes are independent of the electron energy and of the
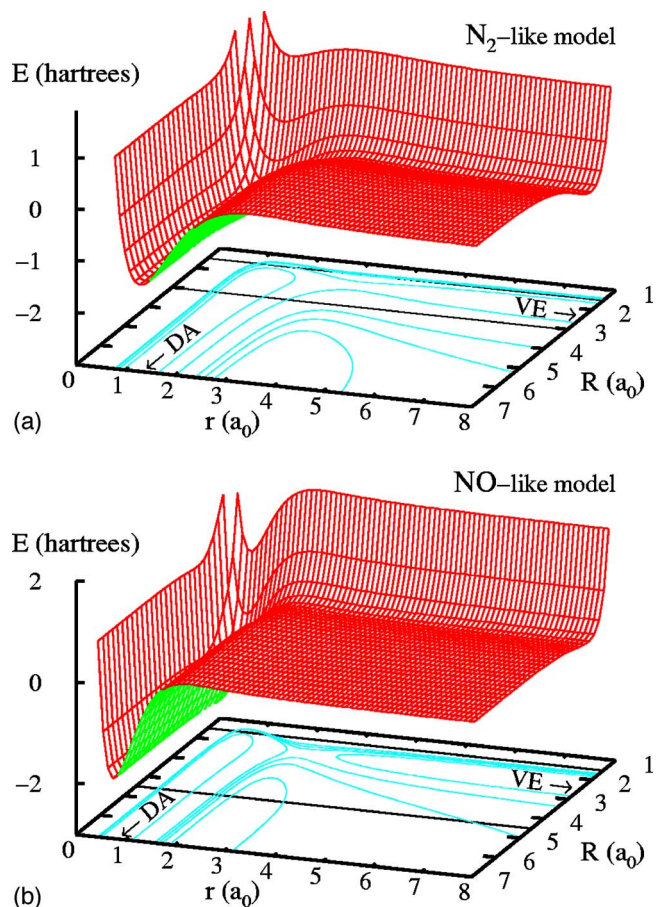


FIG. 2. (Color online) Two-dimensional potential $V(R,r)$ from Eq. (5) for the $N_2$-like (upper panel) and NO-like (lower panel) models. Internuclear distances are given in units of Bohr radius, $a_0 = 5.291\,772\,1 \times 10^{-11}$ m. Energies are in units of hartrees, where 1 hartree $= 4.359\,748 \times 10^{-18}$ J.

vibrational excitation channel. They are determined from the resonance width according to

$$\zeta_v(R) = \sqrt{\frac{\Gamma(R)}{2\pi}}. \qquad (41)$$

However, this expression for the entry amplitude produces an obviously incorrect threshold behavior in the calculated cross sections, with the cross section in the elastic channel diverging as $k_{ei}\to 0$, for example. Therefore an *ad hoc* "barrier penetration factor" [7,18] was introduced to force the correct threshold behavior. The amplitude $\zeta_v(R)$ is then given by

$$\zeta_v(R) = \gamma_v^{l+1/2}(R)\sqrt{\frac{\Gamma(R)}{2\pi}}, \qquad (42)$$

where

$$\gamma_v(R) = \begin{cases} \dfrac{k_v}{k(R)} & \text{if } k_v < k(R), \\[2mm] 1 & \text{if } k_v \geq k(R), \end{cases} \qquad (43)$$
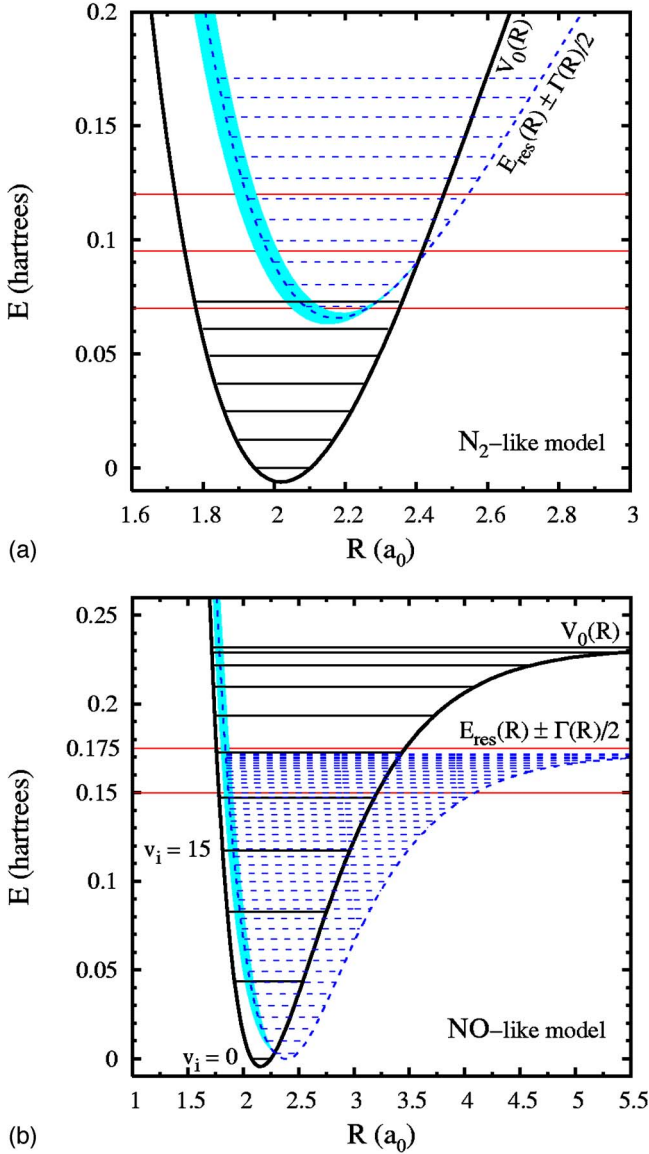
FIG. 3. (Color online) Adiabatic potential curves used in LCP approximation calculations for the $N_2$-like model (upper panel) and the NO-like model (lower panel) with only some vibrational states plotted. Energies $E$ are in units of hartrees and internuclear distances $R$ are in units of $a_0$. Shaded areas illustrate the width $\Gamma(R)$ associated with the complex anion potentials.

$$\frac{k^2(R)}{2} = E_{\text{res}}(R) - V_0(R), \qquad (44)$$

and $k_v$ is the electron momentum in the vibrational channel $v$.

We used both expressions for the entry amplitudes, Eqs. (41) and (42), to calculate the vibrational excitation and dissociative attachment cross sections for comparison with the exact cross sections for the $N_2$-like and NO-like parametrizations of the two-dimensional (2D) model described in following section.

## V. TWO-DIMENSIONAL MODELS FOR ELECTRONIC COLLISIONS WITH $N_2$ AND NO

In order to investigate validity of the LCP approximation we constructed two models, the fixed-nuclei potentials of which are quantitatively similar to adiabatic potential energy curves that have been used in LCP calculations of resonant electronic collisions with the molecules $N_2$ and NO. The local complex potential approximation reproduces the experimental vibrational excitation cross sections reasonably well in the case of the $e^- + N_2$ system [7,8], and so we begin by comparing the exact solutions of our two-dimensional model problem using $N_2$-like potentials with the corresponding LCP approximation to the nuclear dynamics.

Unlike the well-studied $N_2$ system, nuclear motion during electronic collisions with the NO molecule has been investigated in theoretical calculations only recently [19,20]. The lowest-energy resonance in NO (which has $^3\Sigma^-$ symmetry) is fundamentally different from the $^2\Pi_g$ resonance of $N_2$, because the anion potential crosses that of the neutral molecule near its equilibrium internuclear distance. The threshold for vibrational excitation is therefore quite low. Additionally, dissociative attachment proceeds via the same resonance, and regions where the local width is very large are important for this process.

Thus, there is ample reason to suspect that either nonlocal effects or non-Born-Oppenheimer effects might play an important role in this case. In the existing calculations on vibrational excitation and dissociative attachment to this system [19,20], the LCP approximation was employed, generalized using the barrier penetration factor and a nonlocal imaginary part of the molecular anion potential. It is interesting therefore to explore this case with our two-dimensional model and to compare its exact solution with the corresponding LCP approximation, with and without the *ad hoc* barrier penetration factor.

### A. Parametrization of the models for $N_2$ and NO

We used the same functional forms for both systems for the functions $V_0(R)$, $\lambda(R)$, and $\alpha(R)$ appearing in Eqs. (5) and (6),

$$V_0(R) = D_0(e^{-2\alpha_0(R-R_0)} - 2e^{-\alpha_0(R-R_0)}), \qquad (45)$$

$$\lambda(R) = \lambda_\infty + \frac{\lambda_0}{1 + e^{\lambda_1(R-R_\lambda)}}, \qquad (46)$$

$$\lambda_0 = (\lambda_c - \lambda_\infty)(1 + e^{\lambda_1(R_c-R_\lambda)}), \qquad (47)$$

$$\alpha(R) = \alpha_c. \qquad (48)$$

In Eq. (47) $\lambda_0$ is given by the condition at the crossing point of potential curves $\lambda(R_c) = \lambda_c$. In the $N_2$-like model we adjusted the parameters to approximately reproduce the *ab initio* data of Ref. [21] for the $^2\Pi_g$ resonance state of $N_2^-$. In the NO-like model we adjusted the parameters to approximate the data of Ref. [20] for the $^3\Sigma^-$ resonance state of NO$^-$. The numerical values of all the parameters of the two models are listed in Table I.

It should be noted here that this simple parametrization of the $N_2$-like model was optimized for the internuclear distances where resonant vibrational excitation takes place, roughly $1.6a_0 \lesssim R \lesssim 3.0a_0$. That parametrization produces the incorrect behavior as $R \to \infty$, giving a positive electron affinity for the N atom. But the threshold for dissociative attachment in this model ($\sim 0.6$ hartrees) is high above the energy region where resonant vibrational excitation takes place and thus this deficiency of the $N_2$-like potentials is not relevant to our study. On the other hand, in the NO-like model we will study both vibrational excitation and dissociative attachment, and therefore we adjusted parameters to get the correct electron affinity for oxygen and simultaneously the correct position of the crossing point.

The resulting two-dimensional potentials $V(R,r)$ for the $N_2$-like and NO-like models are shown in Fig. 2. In both cases, an incoming electron tunnels through the potential barrier located roughly between $r=2a_0$ and $3a_0$ and is captured into the deep potential well parallel to the $R$ axis for $r<2a_0$. A temporary molecular anion then evolves in this well until the electron is released through the barrier again or the anion dissociates.

The corresponding adiabatic potential curves used in the LCP approximation are shown in Fig. 3. The curves labeled $V_0(R)$ are the potential energies of the neutral molecules. For clarity, only a few vibrational states (0-6 for $N_2$ and 0, 5, 10, ..., 50 for NO) are shown. The potential of the molecular anion is complex for $R<R_c$, and the the width $\Gamma(R)$ is illustrated by the shaded area around the real part $E_{res}(R)$ of the potential.

### B. Wave functions

Before we compare the exact cross sections of vibrational excitation and dissociative attachment with those calculated within LCP approximation, we will examine some examples of scattered wave functions $\Psi_{sc}(R,r)$ [the solutions of Eq. (14)]. These wave functions demonstrate the nature of the resonant collision and directly illustrate the coupling between nuclear and electronic motion.

In Fig. 4 we plot the squared modulus of the scattered wave functions $|\Psi_{sc}(R,r)|^2$ calculated in the $N_2$-like model for the molecule initially in the ground vibrational state and for incoming electron energies $E_{ei}=0.07$, 0.095, and 0.12 hartrees. In this case those are the same as the total energies of the colliding system, because we set the zero of energy to coincide with the ground vibrational state of the molecule, and they are marked by the horizontal lines in Fig. 3.

Although these wave functions describe the system in a time-independent picture, we can see in them the sequence of events that constitutes the resonant behavior of the colliding system. An electron is captured by the molecule, creating a temporary state of the molecular anion, as indicated by the peaks in $|\Psi_{sc}(R,r)|^2$ close to the $R$ axis. The temporarily bound electron described by each of these wave functions can decay back into the continua of the vibrational excitation channels, and that process corresponds to the ridges reaching out to large values of $r$ for $R<R_c=2.405a_0$.
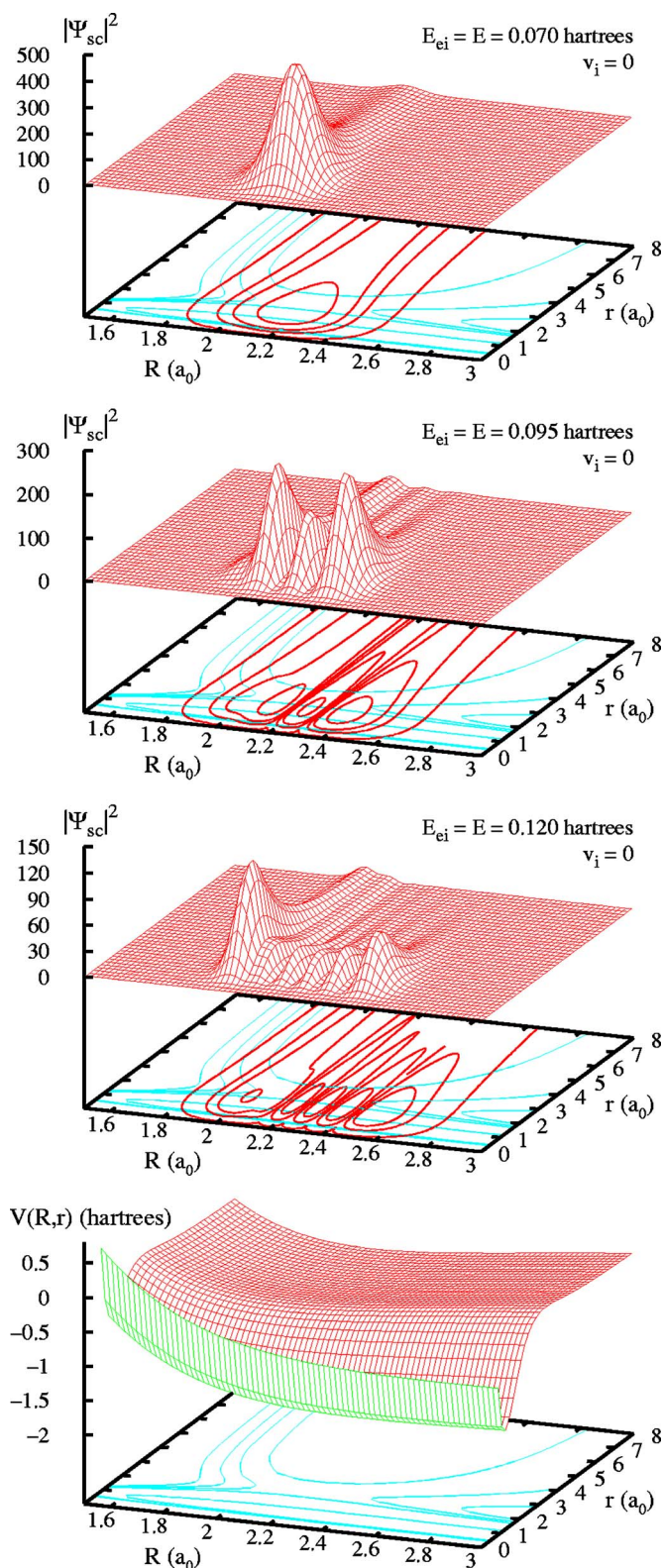


FIG. 4. (Color online) Squared modulus of scattered wave functions, $|\Psi_{sc}(R,r)|^2$ ($R$ and $r$ are in units of $a_0$), for the $N_2$-like model with initial vibrational state $v_i=0$ at the energies of the incoming electron $E_{ei}=0.07$, 0.095, and 0.12 hartrees. The potential $V(R,r)$ (in units of hartrees) in the same region is shown in the bottom panel.

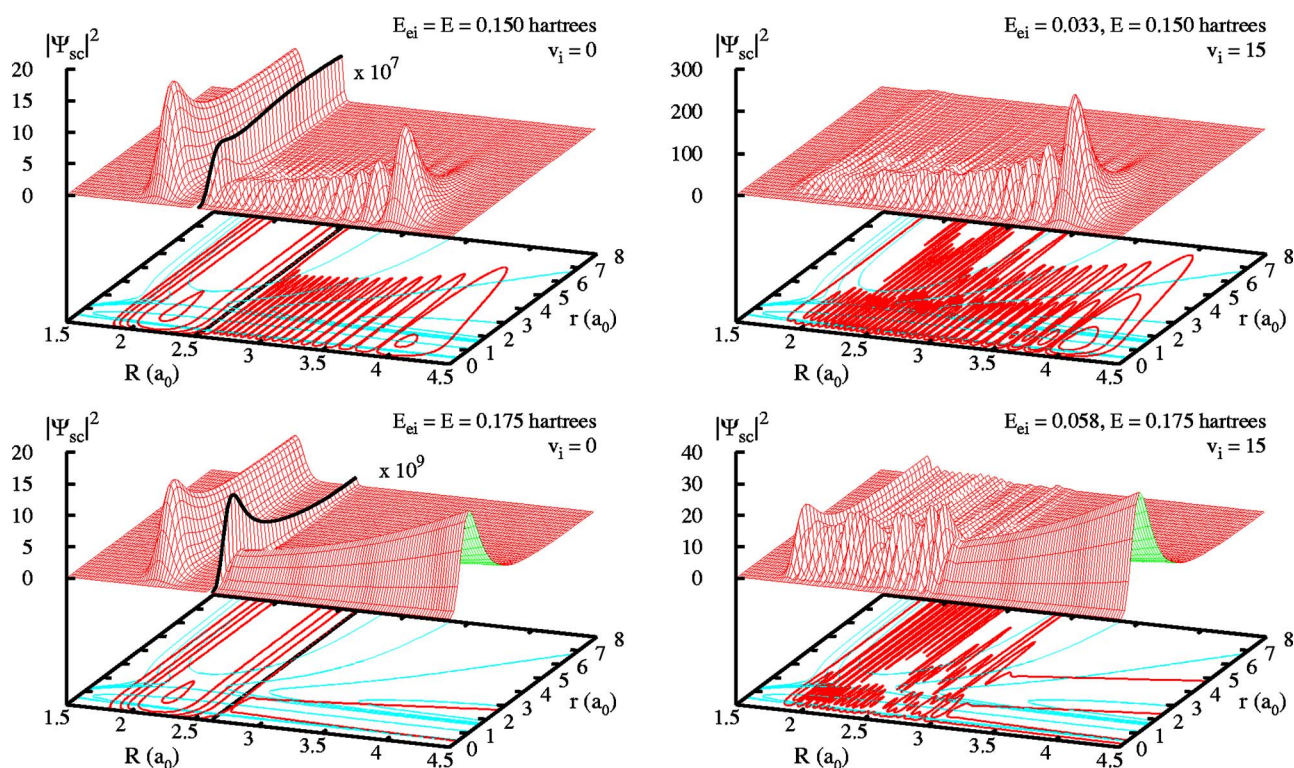FIG. 5. (Color online) Squared modulus of scattered wave functions, $|\Psi_{sc}(R,r)|^2$ ($R$ and $r$ are in units of $a_0$), for the NO-like model for two initial vibrational states ($v_i=0$ and 15) at total energies of $E=0.150$ and 0.175 hartrees (also marked in Fig. 3, lower panel). The wave functions for initial state $v_i=0$ were magnified by $10^7$ at $E=0.15$ hartrees and $10^9$ at $E=0.175$ hartrees for $R \gtrsim 2.5a_0$ (beyond the dark line).

The number of peaks in the wave function at a given energy can be understood by considering nuclear motion in the effective local potential for the temporary molecular anion. We can see that relationship by comparing the nearest quasi-bound state of the molecular anion potential ($E_{res}$ in the upper panel of Fig. 3) that lies below the energy of the colliding system with the two-dimensional scattered wave function. The number of peaks in $|\Psi_{sc}(R,r)|^2$ in these figures is exactly what one would expect based on that comparison, i.e., it is equal to the number of vibrational states supported by $E_{res}(R)$ below the collision energy. In the case of the wave function for $E_{el}=0.12$ hartrees, for example, the nearest state of the anion below the collision energy is $\nu=6$, and there are six peaks in this region of the wave function. The same comparison explains the number of peaks seen in the other panels of Fig. 4. However, it is important to note that the resulting vibrational excitation cross sections cannot be explained as arising from only a single quasibound vibrational state of the anion. If that were the case, the peaks in all the vibrational excitation cross sections would occur at essentially the same energies, but they depend on the final vibrational state, as we will see below.

In the case of the NO-like model, the wave functions at lower energies are very similar to the wave functions of the N$_2$-like model. However, at higher energies this system can undergo dissociative attachment as well as vibrational excitation. In Fig. 5 we show examples of wave functions at total energies just below and just above the dissociative attachment threshold for two initial vibrational states of the molecule, $v_i=0$ (left panels) and $v_i=15$ (right panels). The upper

panels show the squared modulus of the scattered wave functions at total energy $E=0.15$ hartrees, which is below the dissociative attachment threshold. The lower panels show $|\Psi_{sc}(R,r)|^2$ at a total energy of $E=0.175$ hartrees, which is slightly above the dissociative attachment threshold where the cross section is near its maximum value. The total energies for these plots are also marked in the lower panel of Fig. 3. Note that for fixed total energies, the energy of the incoming electron is different depending on the initial vibrational state, and that the scattered wave functions for the molecule in the initial state $v_i=0$ are magnified by factors of $10^7$ and $10^9$ for $R \gtrsim 2.5a_0$.

In the upper panels of Fig. 5 we can clearly see that, when the total energy of the system is below the dissociative attachment threshold, the wave function is restricted in the $R$ direction to the well of the adiabatic molecular anion potential energy curve $V_{res}(R)$, because only vibrational excitation channels are open. Once again the number of peaks in that region of the wave function can be understood by comparing it with the nearest quasibound vibrational state of the molecular anion below the scattering energy. In contrast, in the lower panels where the total energy is above the dissociative attachment threshold, an outgoing wave in $R$ appears which corresponds to dissociation of the molecular anion.

The magnitude of the wave function in the dissociative attachment channel at a given total energy of the system depends strongly on the initial vibrational state, $v_i$, of the molecule and increases by several orders of magnitude with increasing $v_i$. This behavior can be understood qualitatively with a simple and general classical picture of nuclear motion.
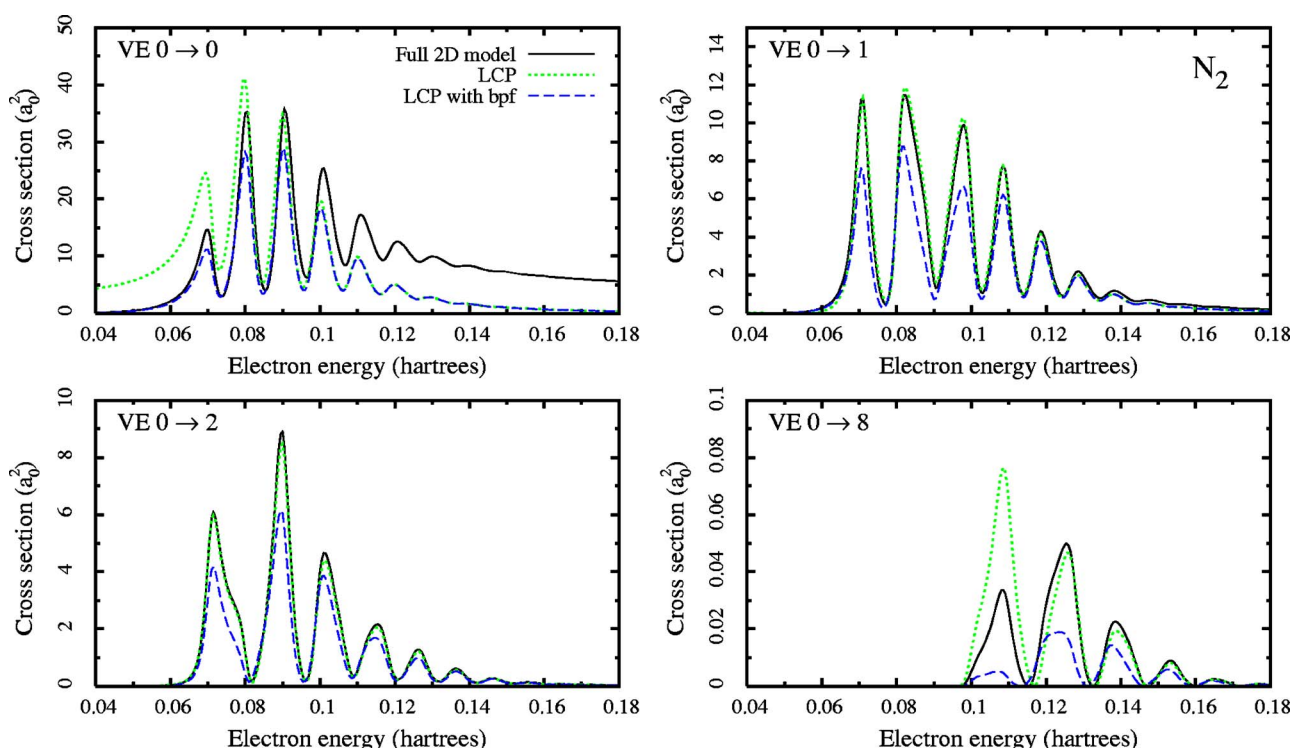
FIG. 6. (Color online) Cross sections (in units of $a_0^2$) for vibrational excitation calculated for the N$_2$-like model. Energies are in units of hartrees. Exact cross sections (solid curves) for the elastic ($v_f=0$) and three inelastic ($v_f=1,2,8$) processes are compared with cross sections in the LCP approximation without (dotted curves) and with (dashed curves) the barrier penetration factor.

If a molecule is in a higher initial vibrational state before the collision with the electron, the kinetic energy of the nuclei is also higher and the temporary molecular anion can most probably escape from the region where electron can be detached (the region where $\Gamma(R)$ is not zero). This increase of the magnitude of the wave function in the dissociative attachment channel is reflected, as we will see in the following section, in a dramatic increase of the dissociative attachment cross section for higher initial vibrational states of the molecule.

### C. Cross sections

Our goal here is to compare the cross sections obtained in these exact calculations with those computed in the LCP approximation, both with and without the barrier penetration factor in its standard form as given in Eqs. (42)–(44). In Fig. 6 we show the cross sections for vibrational excitation in the N$_2$-like model from the ground state, $v_i=0$, to final vibrational states $v_f=0$ (elastic), 1, 2, 8. In Fig. 7 we plot the same vibrational excitation cross sections for the NO-like model. Each plot shows the exact cross section together with both versions of the LCP approximation to it.

For the case of the N$_2$-like model, the exact cross sections are both qualitatively and quantitatively similar to the physical cross sections for this system. The LCP approximation gives nearly exact cross sections for the vibrational excitation of the low lying vibrational states, $v_f=1,2$, but fails badly in describing the first peak for $v_f=8$ which is at an energy where the dynamics can probe the region of the cross-

ing between the anion and neutral potentials. It is at these energies that one expects nonlocal, and possibly nonadiabatic, effects become important.

For elastic scattering we see in the top left panel of Fig. 6 that the LCP approximation fails at low energies, where one might expect it to, because of its intrinsically incorrect threshold energy dependence. Indeed, the barrier penetration factor which was originally designed [18] to force the correct threshold behavior provides a much improved description of the first two peaks in the elastic scattering cross section. At higher incident energies the LCP approximation with and without the barrier penetration factor gives the same results, because the barrier penetration factor tends to unity as one can see in Eq. (43). The disagreement with the exact elastic cross section in this case is due to the nonresonant (background) contribution to this cross section which is not described at all by the LCP approximation.

However the deficiencies of this *ad hoc* correction can easily be seen in the other panels of Fig. 6. Applied to vibrationally inelastic scattering the barrier penetration factor uniformly worsens the agreement between the LCP approximation and the exact cross sections.

One can make qualitatively similar observations about the vibrational excitation cross sections in the NO-like model. Once again the exact solution of the two-dimensional model gives cross sections that are similar to the physical ones for this system. However, in this case the fact that the crossing between the neutral and anion potentials (shown in Fig. 3) occurs near the minimum of the neutral potential curve leads to much poorer agreement in general between the LCP approximation and the exact cross sections. The LCP approxi-
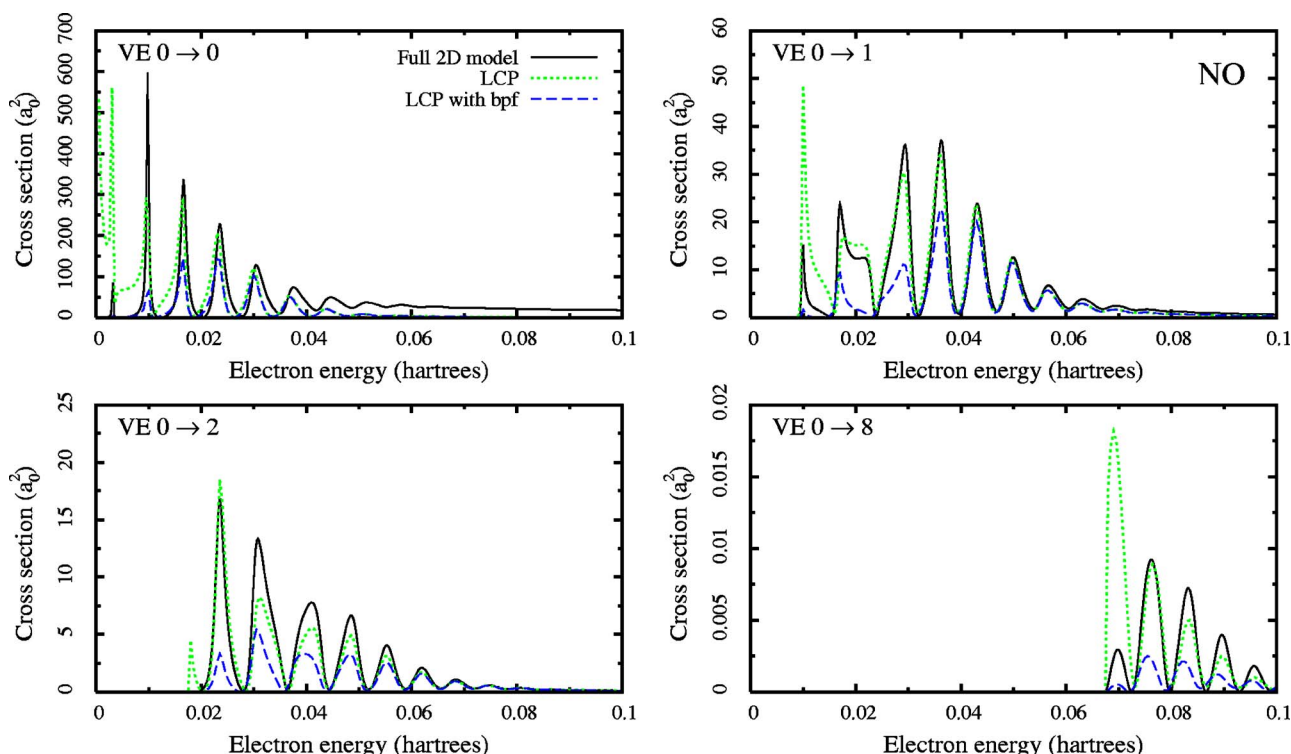
FIG. 7. (Color online) As in Fig. 6, but for the NO-like model.

mation fails for the lower peaks of all the vibrational excitation cross sections, and the barrier penetration factor generally makes the agreement worse.

The dissociative attachment cross sections for this system are shown in Fig. 8. Here we plot the cross section for dissociative attachment to the molecule in initial vibrational states $v_i = 0$, 10, 15, and 20. The magnitude of the cross section increases rapidly with increasing initial vibrational state $v_i$. A simple explanation for that increase was given in the previous subsection in terms of the wave functions at these energies.

The agreement of the cross sections computed using the LCP approximation with the exact 2D model results depends dramatically on the initial state of the system. For low initial vibrational states the LCP approximation gives cross sections that are larger than the exact ones by several orders of magnitude. In these cases the failure of the LCP approximation is probably due to the fact that, at these high incident energies, a vertical transition to the resonant state is unlikely. For that reason, at least nonlocal, and possibly nonadiabatic, effects are playing a dominant role.

For vibrational states in the range of $v_i = 10–15$, the LCP approximation gives quite a good description of the cross sections for dissociative attachment. In this region of intermediate energy for the incident electron it appears that nonlocal or nonadiabatic effects are unimportant. For still higher initial vibrational states, in the range $v_i \gtrsim 15$, the LCP approximation begins to fail near threshold, and ultimately becomes less accurate at higher energies as well, as shown in the lower right panel of Fig. 8. The standard barrier penetration factor further worsens the agreement in all of these cases. For these highly excited initial vibrational states of the

molecule both nonlocal and nonadiabatic effects can be suspected as the reason for the breakdown of the LCP approximation—in particular near the threshold for the dissociative attachment process.

## VI. CONCLUSION

In this paper we have described a complete two-dimensional model for electron scattering from a diatomic molecule that contains the essential physics of resonant electronic collisions and the processes that arise from them. We showed how this model can be used to mimic specific molecular systems and compared it with the local complex potential approximation to nuclear dynamics in metastable electronic states. These are the necessary first steps to constructing a theoretical laboratory with which the underlying assumptions of the powerful class of nonlocal theories for resonant vibrational excitation and dissociative attachment can be tested.

To take the next steps towards doing those tests, we first observe that by using the FEM DVR representation of all the operators we can construct any projection operator to arbitrary precision. We will need the Feshbach projection operator corresponding to any discrete approximation to the resonant state. For example if the approximation to the resonant state is $\psi_{res}(r;R) = \langle r | \psi_{res}(R) \rangle$, depending on the nuclear coordinate $R$ parametrically, the corresponding Feshbach $Q$ projection operator appearing in the nonlocal theories [9] is

$$Q(R) = |\psi_{res}(R)\rangle\langle\psi_{res}(R)|. \qquad (49)$$

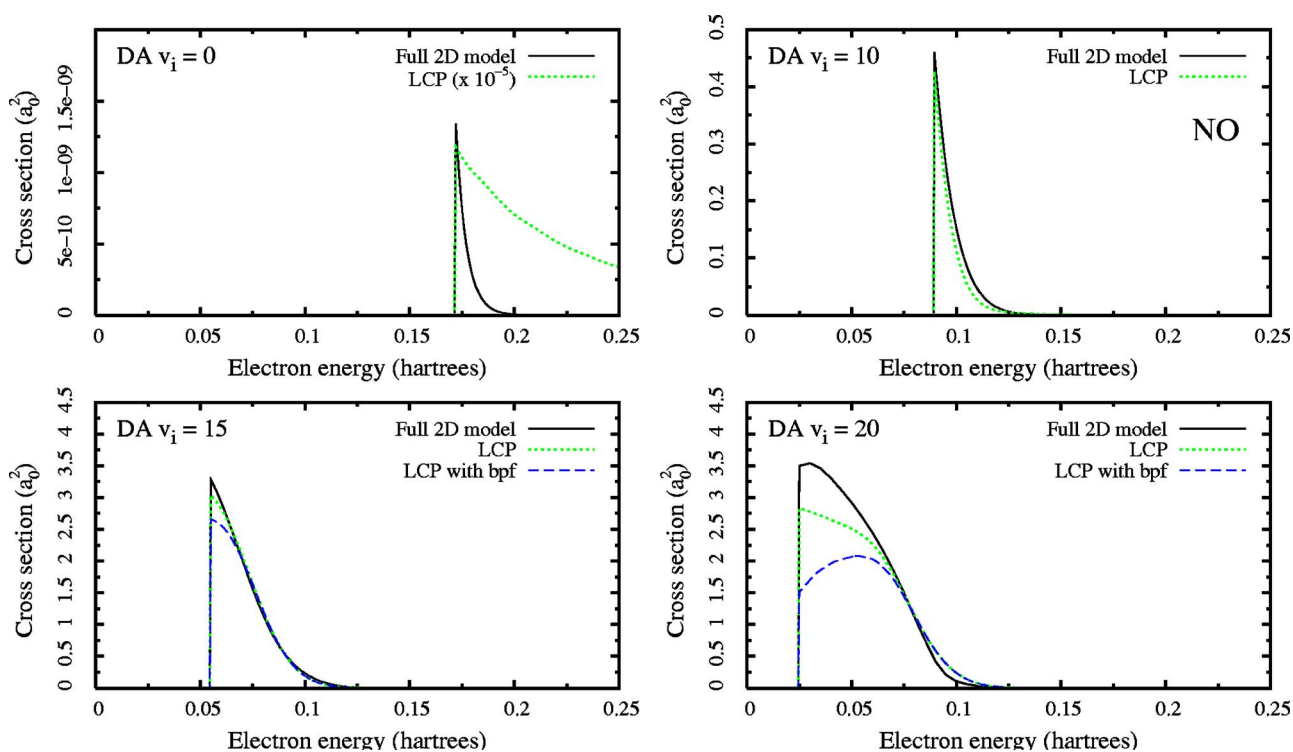In the FEM DVR representation it would be the matrix

FIG. 8. (Color online) Cross sections (in units of $a_0^2$) for dissociative electron attachment for the initial vibrational states $v_i=0$, 10, 15, and 20. Energies are in units of hartrees. Exact cross sections (solid curves) of the 2D model are compared with cross sections obtained by LCP approximation without (dotted curves) and with (dashed curves) the barrier penetration factor. The barrier penetration factor does not change the cross sections in the upper panels.

$$Q_{r_i,r'_j,R_k,R_l} = \sqrt{w_i w_j}\,\psi_{\text{res}}(r_i;R_k)\psi_{\text{res}}(r_j,R_k)\delta_{k,l}, \qquad (50)$$

which is diagonal in the indices corresponding to the nuclear coordinates but nondiagonal in the indices corresponding to the electronic coordinates. The factor of $\sqrt{w_i w_j}$ is a product of DVR weights [14,16] that appears here because the projection operator is nonlocal. The representation of $P=1-Q$ is obviously similar.

The full Hamiltonian operator in Eq. (3) has a completely nondiagonal matrix represension, while the electronic Hamiltonian in Eq. (8) has a FEM DVR matrix representation that is nondiagonal in electronic coordinates but diagonal in nuclear coordinates. The construction of the operators *PHP*, *QHQ*, and *PHQ* is thereby reduced to simple matrix multiplications. When the full Hamiltonian is used, the action of the nuclear kinetic energy is included and all nonadiabatic terms can be calculated exactly. The Born-Oppenheimer approximation is made when the electronic Hamiltonian is used in these projected operators.

Most importantly, all the the Green's functions appearing in the nonlocal theories, e.g., $(E-PHP+i\epsilon)^{-1}$, can be calcu-

lated using the ECS approach with which we constructed the full Green's function $(E-H+i\epsilon)^{-1}$ here. All the other quantities involved in various versions of the nonlocal theories can be constructed using similar ideas.

Therefore, although we have restricted ourselves here to comparisons with the local complex potential approximation, these tools open the way to comparisons with any form of the nonlocal theories that have been applied to physical systems. The two-dimensional model we described here, together with the associated numerical methods of the ECS and FEM DVR approaches, form a laboratory with which those comparisons can be made. Such calculations will be reported in a subsequent study.

[1] T. F. O'Malley, Phys. Rev. **150**, 14 (1966).

[2] T. F. O'Malley, Phys. Rev. **185**, 101 (1969).

[3] T. F. O'Malley and H. S. Taylor, Phys. Rev. **176**, 207 (1968).

[4] D. T. Birtwistle and A. Herzenberg, J. Phys. B **4**, 53 (1971).

[5] J. N. Bardsley, A. Herzenberg, and F. Mandl, Proc. Phys. Soc. London **89**, 305 (1966).

[6] L. Dubé and A. Herzenberg, Phys. Rev. A **20**, 194 (1979).

[7] A. U. Hazi, T. N. Rescigno, and M. Kurilla, Phys. Rev. A **23**, 1089 (1981).

[8] M. Berman, H. Estrada, L. S. Cederbaum, and W. Domcke, Phys. Rev. A **28**, 1363 (1983).

[9] W. Domcke, Phys. Rep. **208**, 97 (1991).

[10] J. N. Bardsley and J. M. Wadehra, Phys. Rev. A **20**, 1398 (1979).

[11] M. Čížek, J. Horáček, and W. Domcke, J. Phys. B **31**, 2571 (1998).

[12] M. Allan, M. Čížek, J. Horáček, and W. Domcke, J. Phys. B **33**, L209 (2000).

[13] M. Čížek, J. Horáček, A. C. Sergenton, D. B. Popović, M. Allan, W. Domcke, T. Leininger, and F. X. Gadea, Phys. Rev. A **63**, 062710 (2001).

[14] T. N. Rescigno and C. W. McCurdy, Phys. Rev. A **62**, 032706 (2000).

[15] J. V. Lill, G. A. Parker, and J. C. Light, Chem. Phys. Lett. **89**, 483 (1982).

[16] C. W. McCurdy, M. Baertschy, and T. N. Rescigno, J. Phys. B **37**, R137 (2004).

[17] *Handbook of Mathematical Functions with Formulas, Graphs, and Mathematical Tables*, edited by M. Abramowitz and I. A. Stegun (Dover Publications, New York, 1972).

[18] N. Bardsley and J. M. Wadehra, J. Chem. Phys. **78**, 7227 (1983).

[19] Z. Zhang, W. Vanroose, C. W. McCurdy, A. E. Orel, and T. N. Rescigno, Phys. Rev. A **69**, 062711 (2004).

[20] C. S. Trevisan, K. Houfek, Z. Zhang, A. E. Orel, C. W. McCurdy, and T. N. Rescigno, Phys. Rev. A **71**, 052714 (2005).

[21] J. G. Lauderdale, C. W. McCurdy, and A. U. Hazi, J. Chem. Phys. **79**, 2200 (1983).